BMC Medical Imaging

RESEARCH

Open Access

Machine learning model for non-alcoholic steatohepatitis diagnosis based on ultrasound radiomics

Fei Xia[1,3], Wei Wei[2], Junli Wang[3], Yayang Duan[1], Kun Wang[3] and Chaoxue Zhang[1*]

Abstract

Background Non-Alcoholic Steatohepatitis (NASH) is a crucial stage in the progression of Non-Alcoholic Fatty Liver Disease(NAFLD). The purpose of this study is to explore the clinical value of ultrasound features and radiological analysis in predicting the diagnosis of Non-Alcoholic Steatohepatitis.

Method An SD rat model of hepatic steatosis was established through a high-fat diet and subcutaneous injection of CCl_4. Liver ultrasound images and elastography were acquired, along with serum data and histopathological results of rat livers.The Pyradiomics software was used to extract radiomic features from 2D ultrasound images of rat livers. The rats were then randomly divided into a training set and a validation set, and feature selection was performed through dimensionality reduction. Various machine learning (ML) algorithms were employed to build clinical diagnostic models, radiomic models, and combined diagnostic models. The efficiency of each diagnostic model for diagnosing NASH was evaluated using Receiver Operating Characteristic (ROC) curves, Clinical Decision Curve Analysis (DCA), and calibration curves.

Results In the machine learning radiomic model for predicting the diagnosis of NASH, the Area Under the Curve (AUC) of ROC curve for the clinical radiomic model in the training set and validation set were 0.989 and 0.885, respectively. The Decision Curve Analysis revealed that the clinical radiomic model had the highest net benefit within the probability threshold range of > 65%. The calibration curve in the validation set demonstrated that the clinical combined radiomic model is the optimal method for diagnosing Non-Alcoholic Steatohepatitis.

Conclusion The combined diagnostic model constructed using machine learning algorithms based on ultrasound image radiomics has a high clinical predictive performance in diagnosing Non-Alcoholic Steatohepatitis.

Keywords Non-Alcoholic Steatohepatitis, Radiomics, Ultrasound, Machine Learning

Introduction

NAFLDis the most common chronic liver disease in humans, and its prevalence continues to rise [1].NAFLD comprises Non-Alcoholic Fatty Liver (NAFL) and NASH [2].NASH is considered a progressive form of NAFLD, characterized by liver fat deposition, inflammation, hepatocyte injury, and varying degrees of fibrosis. It is associated with disease progression, the development of cirrhosis, and the need for liver transplantation.It is estimated that 20% of NASH patients will progress to cirrhosis. The mortality rate among NASH patients is

*Correspondence:
Chaoxue Zhang
zcxay@163.com
[1] Department of Ultrasound, The First Affiliated Hospital of Anhui Medical University, No.218 Jixi Road, Shushan District, Hefei 230022, Anhui, China
[2] Department of Ultrasound, The First Affiliated Hospital of Wannan Medical College (Yijishan Hospital), NO.2 Zheshan West Road, Wuhu 241000, China
[3] Department of Ultrasound, WuHu Hospital, East China Normal University (The Second People's Hospital, WuHu), No.259 Jiuhuashan Road, Jinghu District, Wuhu 241001, Anhui, China

significantly higher than that of the general population or non-inflammatory subtypes of NAFLD patients. Despite its significance, NASH remains insufficiently understood in clinical practice [3, 4].

For a long time, the majority of research efforts have primarily focused on viral hepatitis and liver fibrosis, with limited reports on NAFLD. However, early and accurate diagnosis of NASH is beneficial for halting or reversing the progression of NAFLD [5].Percutaneous liver biopsy has been considered the gold standard method for staging fat deposition and fibrosis. However, it has several drawbacks, including invasiveness, the risk of bleeding, the potential for sampling errors due to the heterogeneity of disease distribution, and it may not be readily accepted by patients and their families [6, 7].Currently, non-invasive methods for detecting and assessing NAFLD in clinical practice include CT, MRI, and ultrasound. However, none of these methods can detect NASH specifically. CT involves ionizing radiation, and MRI is expensive. Both of these methods have limitations in their clinical application, making them challenging to use extensively [8, 9]. Hence, there is an urgent need for a reliable, convenient, and non-invasive diagnostic tool for assessing liver fat deposition.

In the field of imaging techniques, some studies have indicated a correlation between the grading of fat deposition obtained through abdominal ultrasound and the risk of developing NASH [10, 11].Radiomics, on the other hand, can detect extremely subtle regional changes and analyze the overall condition of an organ or tissue, making it suitable for assessing the extent and severity of diffuse conditions like liver fat deposition [12].In this study, we based our research on the "two-hit hypothesis" for the development of NASH and utilized a combined model of high-fat diet (HFD) feeding and CCl4 administration as proposed by Kubota and others [13, 14].We employed a rat liver injury model that closely resembles human NAFLD by inducing liver damage through a combination of HFD feeding and CCl4 administration, following the approach outlined in references [15, 16].We hypothesized that by categorizing rats based on the histopathological results of liver inflammation and using radiomics to extract additional quantitative feature information from NASH ultrasound images, combined with relevant clinical parameters, we could generate a joint detection model for NASH, thereby improving NASH detection.

Materials and methods

Animal model

This study was approved by the Clinical Medicine Research Ethics Committee of the First Affiliated Hospital of Anhui Medical University, China, and complies with the National Guidelines for Animal Care and Use in China. Ethics approval number: 5101114.Ninety male SD rats (initial weight: 140-170g) were selected. Choosing male SD rats was to avoid hormonal fluctuations, as female rats undergo hormonal fluctuations during their estrous cycles, which could potentially affect experimental outcomes.After a three-day adaptation period and numbering, the rats were randomly divided into two groups: a normal control group consisting of 30 rats fed a standard diet and a high-fat group consisting of 60 rats fed a high-fat diet.The high-fat diet with the following nutritional composition: 20% protein, 20% carbohydrates, and 60% fat.The high-fat group was administered a mixture of CCl4 in oil (1:4) from the 8th week until the 14th week (0.2 mL/kg; twice a week; intraperitoneally).In the normal control group, 10 rats were randomly selected at the 4th, 10th, and 14th weeks for imaging examination. In the high-fat group, 10 rats were randomly selected at the 4th, 6th, 8th, 10th, 12th, and 14th weeks after anesthesia for imaging examination. Subsequently, blood samples were collected from the abdominal aorta, and finally, under anesthesia, the rats were euthanized by cervical dislocation, and liver tissue was obtained.

Ultrasound data acquisition

Examination is performed using the ACUSON Sequoia real-time shear wave elastography ultrasound diagnostic system (Brand: Siemens, Origin: USA), equipped with a standard linear array 10L4 transducer (4-10MHz), and an animal experiment-specific V6 ultrasound diagnostic system (Brand: FiNo, Origin: China), equipped with an X4-12L transducer (4-12MHz).Before the examination, all rats had a one-day period of fasting. Anesthesia was initiated by administering pentobarbital sodium by an intraperitoneal injection, using a solution of 3% saline at a dosage of 40mg/kg. Subsequent to undergoing ultrasonic scanning, once anesthetized, the rats' abdominal fur was surgically extracted while they remained immobile on the operating table. The evaluation began with a conventional B-mode ultrasound scan. Following the standard scan, the liver lobes were consistently recorded as bigger two-dimensional images. Afterward, the mode was changed to 2D-SWE and P-SWE in order to get liver lobe elastography data. Utilizing the 2D-SWE mode, the elasticity values of adjacent liver and kidney tissue were ascertained. These results were then used to determine the liver-to-kidney elasticity ratio. The grayscale ultrasonography and SWE findings were stored as duplex pictures in Digital Imaging and Communications in Medicine (DICOM) format for further radiomics investigation.

Blood and tissue sampling

Following the completion of the ultrasound scans, the rats' body weights were measured. Subsequently, blood samples were collected through abdominal aorta puncture, and the rats were euthanized. Blood was collected into anticoagulant tubes, centrifuged at 4000rpm for 15 min, and the serum was stored at -80 °C for later use. Simultaneously, the liver was quickly separated, rinsed with physiological saline, and the central lobe of the liver was fixed in 10% neutral formalin for further processing.

Serum and histopathological analysis

The collected serum samples were labeled and sent to the laboratory at our Hospital for analysis. The serum samples were tested for the following parameters: alanine transaminase (ALT), aspartate transaminase (AST), AST/ALT ratio, gamma-glutamyl transferase (GGT), total cholesterol (CHOL), triglycerides (TG), high-density lipoprotein cholesterol (HDL-C), and low-density lipoprotein cholesterol (LDL-C).

The liver tissue was preserved in a solution of 10% neutral formalin for 24 h and then underwent standard tissue processing. Subsequently, the specimen was treated with hematoxylin and eosin (H&E) to facilitate histological examination. The SAF score system was employed to diagnose NAFLD pathologically. NASH is diagnosed when there is a concurrent presence of ballooning degeneration, hepatic steatosis, and lobular inflammation, with each component scoring 1 point and the total score being ≥ 3 points. Significant fibrosis is characterized by a fibrosis score of F2 or above. Fibrosis scores range from F0 (no fibrosis) to F4 (cirrhosis), with F2 indicating the presence of both peri-sinusoidal and portal/periportal fibrosis, while F3 manifests bridging fibrosis.

Radiomic feature extraction and selection

The ultrasound images were exported from our imaging system.Then, ITK-SNAP 3.8.0 (www.itksnap.org/) was used to delineate the contours of the Region of Interest (ROI) for radiomic feature extraction, model building, and evaluation. Radiomic features were automatically extracted from each image using the "pyradiomics" toolkit.To select radiomic features with good reproducibility and low redundancy, the following steps were taken:①Independent sample t-tests were performed on all extracted features, and features with $p > 0.05$ were removed.②For highly repetitive features, the Pearson correlation coefficient was calculated to express the relationship between features, and only one of any pair of features with a correlation coefficient > 0.9 was retained.③The Least Absolute Shrinkage and Selection Operator (LASSO) algorithm was applied, and ten-fold cross-validation was used to determine the optimal λ value. Based on the model corresponding to the best λ value, non-zero coefficient radiomic features were selected.④All selected features were standardized using the Z-score method.⑤Finally, radiomic features and their corresponding coefficients were selected based on the LASSO algorithm.

Establishment of clinical models, radiomic models, and clinical radiomic models

After feature selection, various machine learning (ML) classification algorithms were used to establish clinical models, radiomic models, and clinical radiomic models. These algorithms included Logistic Regression (LR), Support Vector Machine (SVM), K Nearest Neighbor (KNN), Random Forest (RF), Extremely Randomized Trees (ExtraTree), eXtreme Gradient Boosting (XGBoost), Light Gradient Boosting Machine (LightGBM), and Multi-Layer Perceptron (MLP).Fig. 1 in the analysis pipeline illustrates the workflow for establishing the clinical radiomic model.

Model evaluation

ROC, AUC and DCA were used to evaluate the performance and clinical utility of the radiomic model, clinical model, and clinical radiomic model in both the training and validation sets. Additionally, accuracy, sensitivity, specificity, PPV, and NPV were also assessed.

Statistical analysis

Statistical analysis was conducted using R software (version 4.3.2) and Python (version 3.7.2).Continuous data were evaluated for consistency between the training and validation sets using independent sample t-tests. The performance of the models was evaluated using ROC curves, and the AUC of each prediction model was compared using the DeLong test. The clinical value of various prediction models was compared using DCA. Model fitting was assessed using calibration curves. The calculations for DCA mainly utilized the "rms" and "rmda" packages in R. Statistical significance for all two-tailed tests was set at $P < 0.05$.

Results

Clinical features

Out of the 90 rats, three rats died unexpectedly, leaving a total of 87 rats. The basic clinical information of the rats is presented in Table 1. Among these, 58 rats were diagnosed with NASH, and 29 rats were diagnosed as non-NASH (Fig. 2 shows macroscopic images of rat liver and pathological images under a microscope). These rats were randomly divided into a training set (60 rats) and a validation set (27 rats).

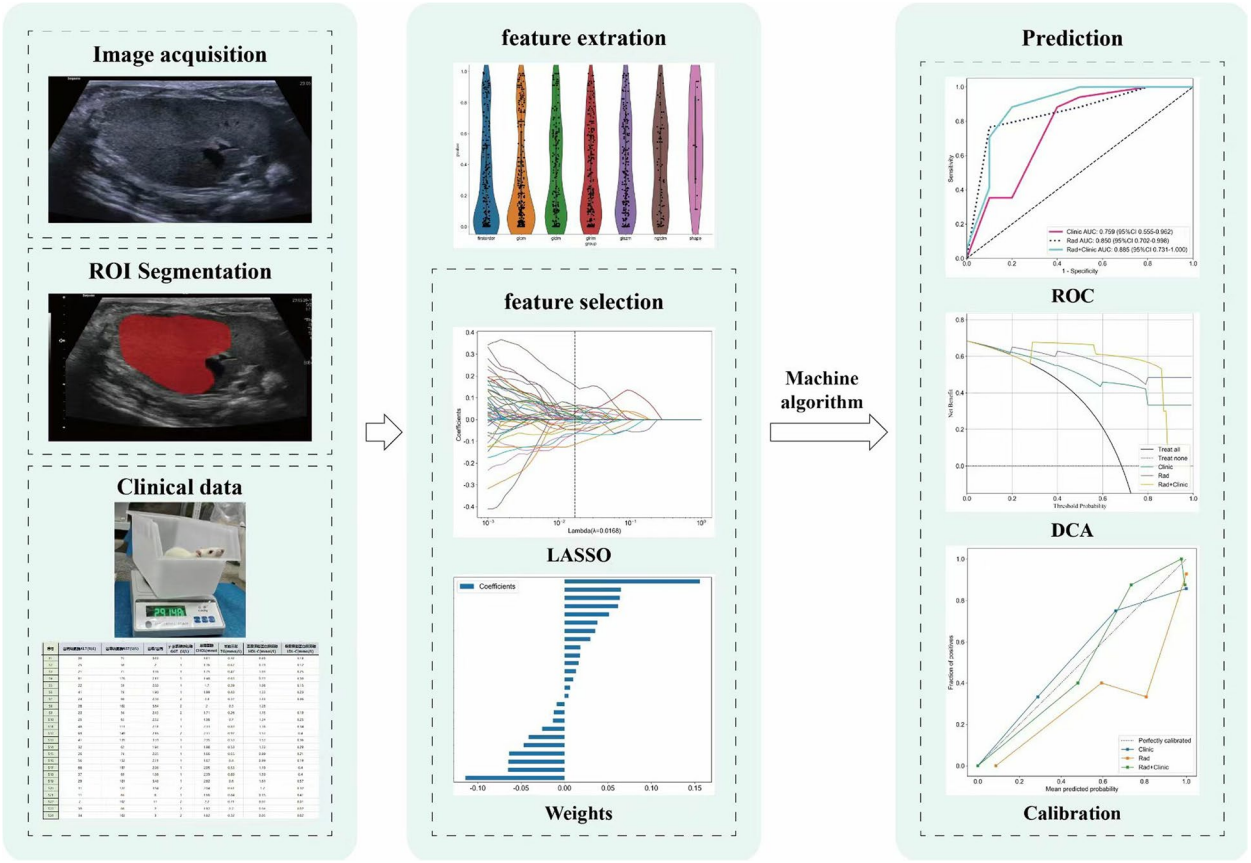

Fig. 1 The overall conceptual process of this study's model.ROI, region of interest; LASSO, least absolute shrinkage and selection operator; ROC, receiver operating characteristic curve; DCA, Decision Curve Analysis

Table 1 Clinical baseline features of rats in the training and validation sets

	Training set	Validation set	*P*
Weight(mean ± SD) (g)	499.17 ± 90.73	524.00 ± 104.41	0.263
ALT(mean ± SD)(u/l)	84.68 ± 126.13	119.04 ± 122.02	0.238
AST(mean ± SD)(u/l)	232.08 ± 256.10	301.67 ± 276.14	0.256
AST/ALT(mean ± SD)	3.77 ± 6.30	2.92 ± 1.47	0.4886
GGT(mean ± SD)(u/l)	2.22 ± 3.18	4.19 ± 5.83	0.050
CHOL(mean ± SD)(mmol/l)	1.85 ± 0.40	1.81 ± 0.45	0.699
TG(mean ± SD)(mmol/l)	0.70 ± 0.28	0.78 ± 0.37	0.258
HDL-C(mean ± SD)(mmol/l)	0.93 ± 0.41	0.90 ± 0.29	0.782
LDL-C(mean ± SD)(mmol/l)	0.29 ± 0.13	0.31 ± 0.16	0.506
PSWE-Vs(mean ± SD)(m/s)	1.09 ± 0.14	1.13 ± 0.19	0.219
PSWE-E(mean ± SD)(kpa)	3.62 ± 0.98	3.97 ± 1.33	0.176
2DSWE(mean ± SD)(kpa)	4.78 ± 1.17	4.93 ± 1.48	0.601
ratio(mean ± SD)	0.85 ± 0.24	0.90 ± 0.25	0.340

The two groups did not show significant differences in various clinical features such as weight ($p = 0.261$), ALT($p = 0.238$), AST($p = 0.256$), AST/ALT ($p = 0.489$), GGT ($p = 0.050$), etc. Therefore, these clinical features were included in the model-building process. The clinical features of the rats were summarized into a shape value plot using the LightGBM algorithm (Fig. 3). The shape value plot indicated that weight, P-SWE-E, and LDL-C played a major role in predicting the diagnosis of NASH in the model.

Selection of radiomic features

A total of 1288 features were extracted from each image, and after feature preprocessing, the remaining 91 features were used for dimension reduction using LASSO algorithm. Finally, a radiomic model was established using the remaining 25 features. Figure 4 displays the feature selection using the LASSO algorithm, and the correlations of various features are shown in Fig. 5.

Construction of clinical model, radiomic model, and clinical radiomic model

Based on the ROC results of various machine learning classification algorithms, a comprehensive comparison of each model's AUC, ACC, sensitivity, specificity, and other

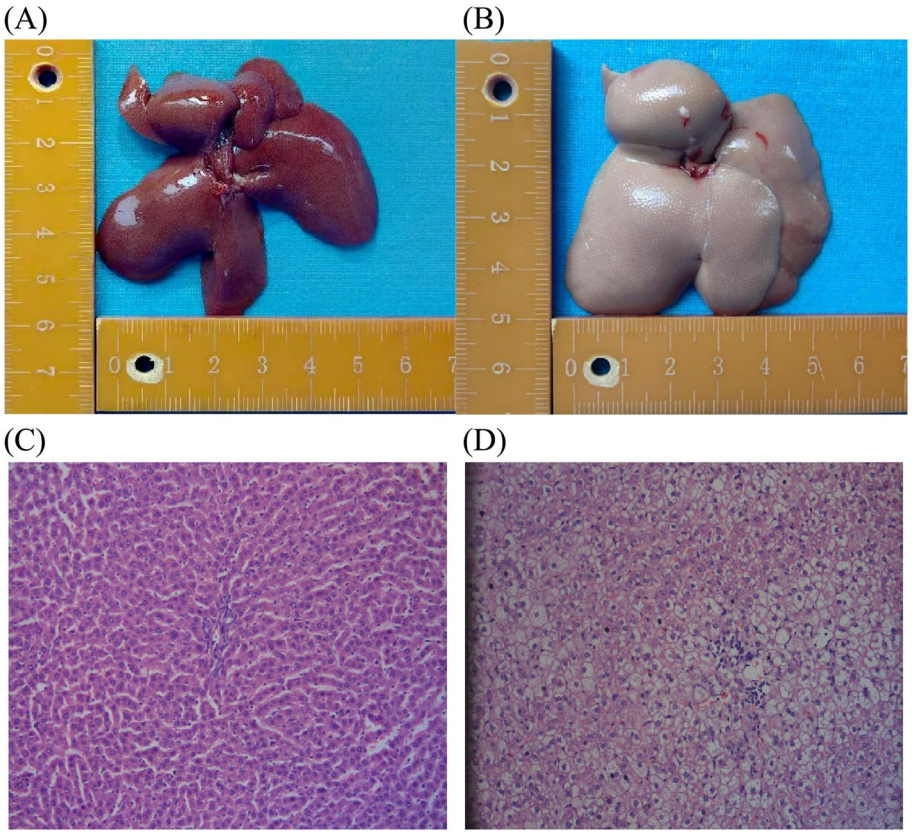

Fig. 2 **A** Gross macroscopic image of a normal rat liver, **B** Gross macroscopic image of a NASH rat liver, **C** Pathological image of normal rat liver tissue (H&Estaining, × 200 magnification), **D** Pathological image of NASH rat liver tissue (H&E staining revealing severe hepatic steatosis, hepatocellular ballooning, and lobular in flammation, × 200 magnification)

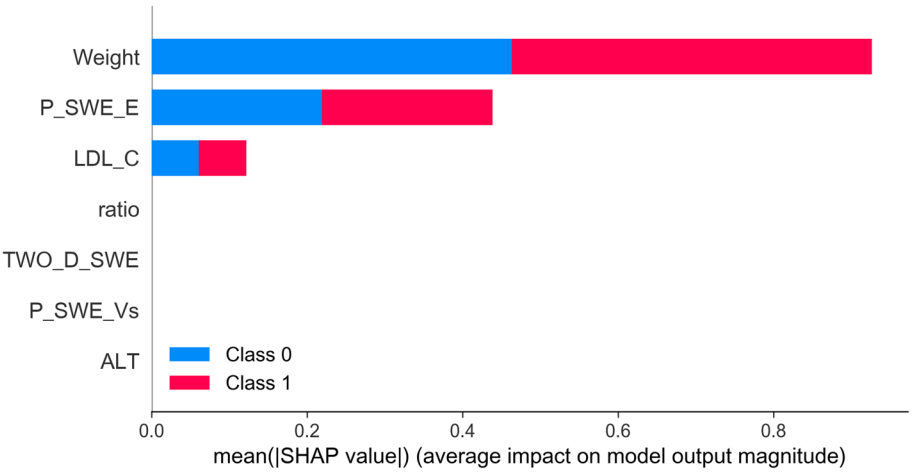

Fig. 3 Shape Value Plot of Clinical Features

indicators was conducted. The ROC results for each machine learning algorithm are shown in supplementary materials. In the end, both the clinical model and the radiomic model were selected to use KNN algorithm, while the clinical radiomic model used the Light GBM algorithm. The ROC results for the three models are presented in Table 2.

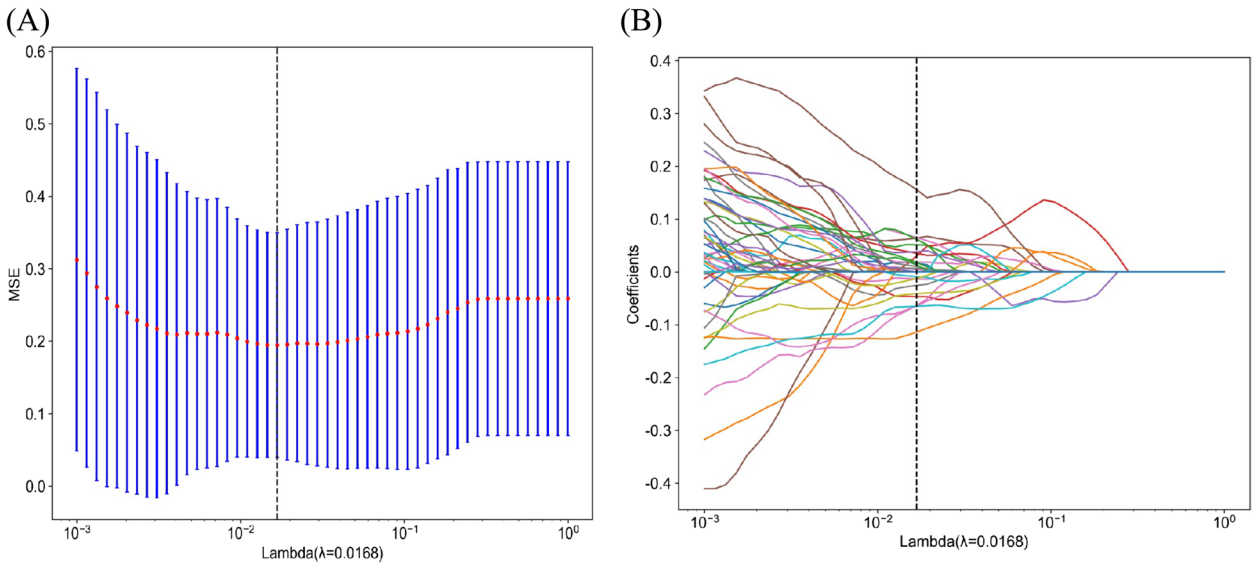

Fig. 4 Using the Least Absolute Shrinkage and Selection Operator (LASSO) regression, a total of 25 key radiomic features were determined. **A** The 25 non-zero coefficients were obtained based on the λ values. **B** LASSO coefficient profiles are plotted against the log (λ) sequence

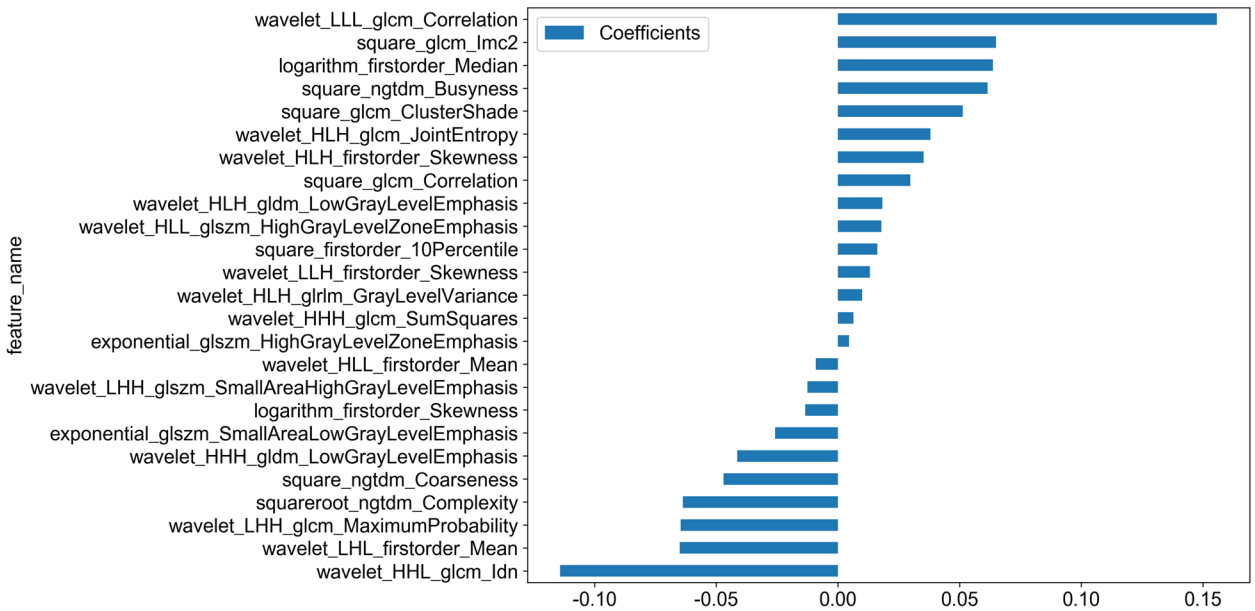

Fig. 5 The 25 features and their coefficients developed for the radiomic model

Model evaluation

The ROC curves for the radiomic model, clinical model, and clinical radiomic model are shown in Fig. 6.According to the DeLong test, the clinical radiomic model outperforms the clinical model in the training set, and the difference is statistically significant ($p=0.013$). However, in the training set, there is no statistically significant difference between the clinical radiomic model and the radiomic model ($p=0.169$). In the validation set, there is no statistically significant difference between the clinical radiomic model and the clinical model ($p=0.369$) or the radiomic model ($p=0.508$).Using DCA, the clinical utility of the models can be directly assessed. Figure 7 shows that if the threshold probability is greater than 65%, using the clinical radiomic model to predict the diagnosis of NASH in this study will result in a greater net benefit. At the same time, the predictive abilities and actual performance of each model were assessed using calibration curves. In the

Table 2 Diagnostic Performance of Radiomic Model, Clinical Model, and Clinical Radiomic Model in the Training and Validation Sets

	AUC(95%CI)	ACC	SEN	SPE	PPV	NPV
Training set						
Radiomics model	0.967 (0.932–1.000)	0.900	0.842	0.927	0.842	0.927
Clinical model	0.900 (0.830–0.969)	0.783	0.947	0.707	0.600	0.967
Clinical radiomics model	0.989 (0.967–1.00)	0.983	0.947	1.000	1.000	0.976
Validation set						
Radiomics model	0.850 (0.702–0.998)	0.815	0.900	0.765	0.692	0.929
Clinical model	0.759 (0.555–0.962)	0.778	0.600	0.882	0.750	0.789
Clinical radiomics model	0.885 (0.731–1.000)	0.852	0.800	0.882	0.800	0.882

Abbreviations: ACC Accuracy, *AUC* Area Under the Receiver Operating Characteristic Curve, *SEN* Sensitivity, *SPE* Specificity, *PPV* Positive Predictive Value, *NPV* Negative Predictive Value

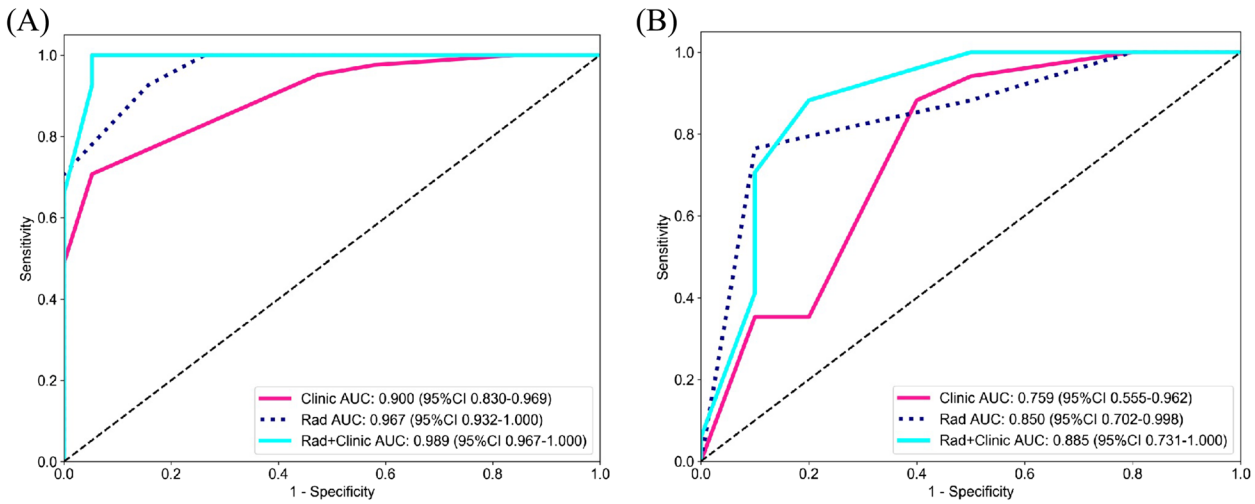

Fig. 6 ROC curves of the radiomics model, clinical model, and clinical-radiomics combined model in the training and validation sets. **A** ROC curves of the three models in the training set. **B** ROC curves of the three models in the validation set

training set, the p-value for the H–L test of the combined model was 0.52, and in the validation set, the p-value for the H–L test of the combined model was 0.83. This indicates that the combined model is highly suitable for both the training and validation sets. Additionally, the calibration curve in the validation set shows that the clinical-radiomics combined model is the best method for diagnosing NASH (Fig. 8).

Discussion

NASH is a crucial stage in the progression of NAFLD, and only NASH patients among those with NAFLD can develop severe conditions such as cirrhosis and liver cancer [17]. Therefore, the early and effective clinical diagnosis of NASH is of significant importance. This study utilized a NAFLD animal model for research. Animal models can provide complete liver tissue samples for

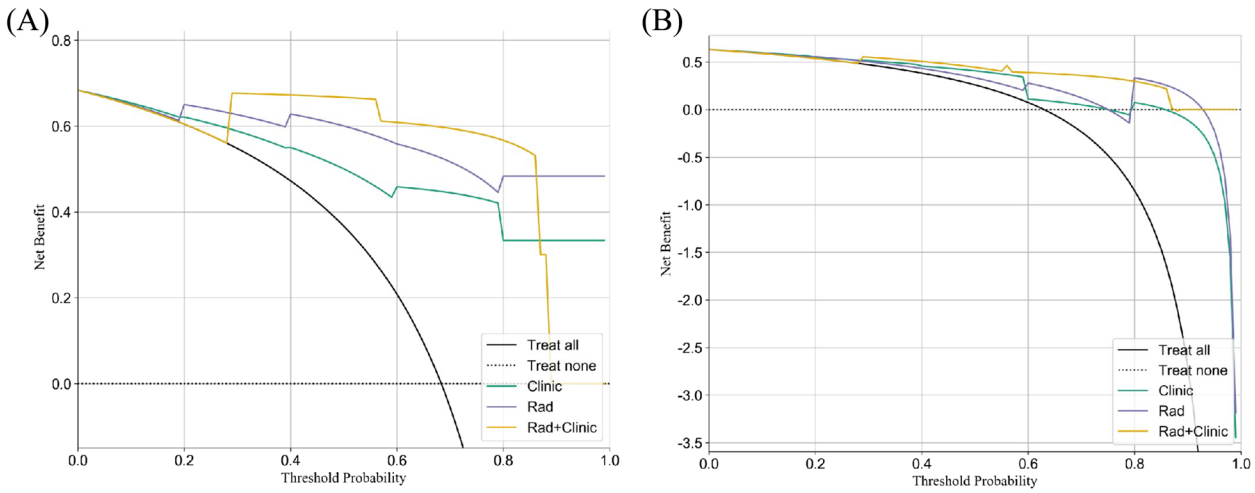

Fig. 7 Decision Curve Analysis (DCA) of the radiomics model, clinical model, and clinical-radiomics combined model in the training and validation sets. **A** DCA of the three models in the training set. **B** DCA of the three models in the validation set

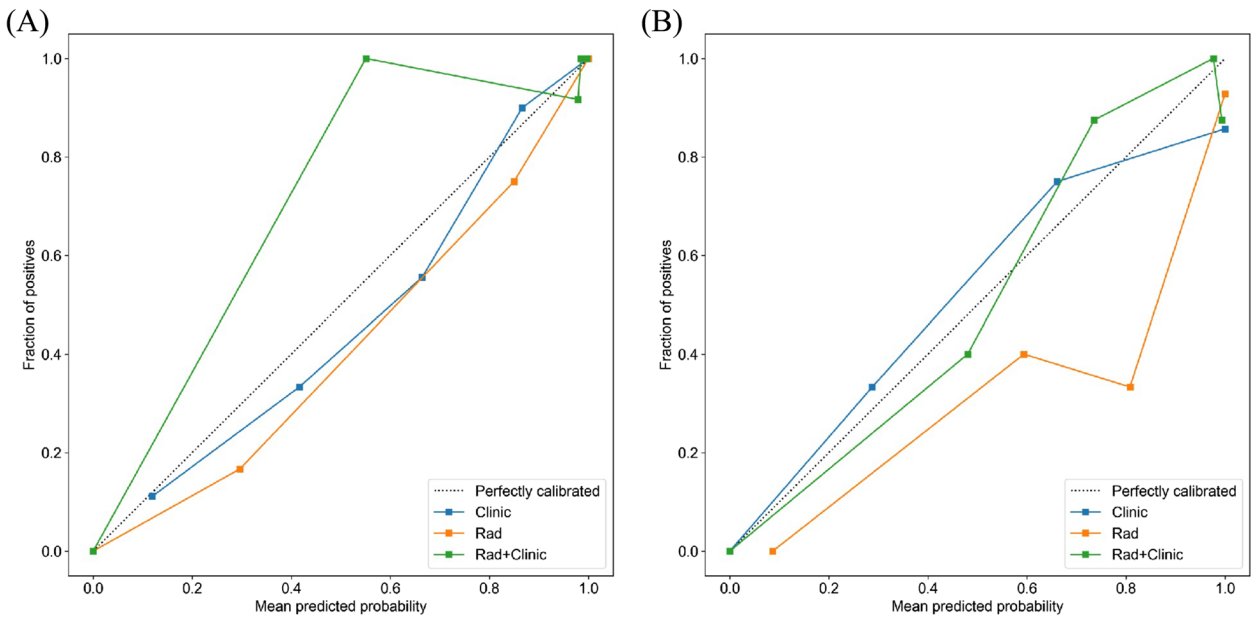

Fig. 8 Calibration curves of the radiomics model, clinical model, and clinical-radiomics combined model in the training and validation sets. **A** Calibration curves of the three models in the training set. **B** Calibration curves of the three models in the validation set

accurate pathological diagnosis, avoiding the limitations of limited tissue sampling and incorrect pathological diagnosis in patients due to biopsy [18].In our study, we established a model of liver fat deposition through a high-fat diet and subcutaneous injection of CCL4. This method partially replicates the development pattern of NAFLD and has been widely used in research [19, 20].

In this study, we utilized ML models due to their ability to handle complex nonlinear relationships between variables and outcomes, surpassing traditional linear prediction models [21].The shape value analysis obtained through the ML LightGBM algorithm revealed that body weight and LDL-C play a primary role in predicting NASH, which aligns with the findings of Vilar-Gomez E's research. They discovered a correlation between weight loss and improvement in histological features of NASH tissue. Additionally, previous studies have indicated that 72% of NASH patients exhibit lipid abnormalities [22, 23].Furthermore, this study highlights the significant value of P-SWE in the non-invasive assessment of NASH.

Recent research has also indicated that measuring liver stiffness using ultrasound elastography may serve as a biomarker for non-invasive diagnosis of fatty liver disease, aligning with the findings presented in this study [24–26].Based on these clinical factors, we established a clinical model, which had an AUC of 0.900 in the training set and an AUC of 0.759 in the validation set.

Radiomics utilizes advanced statistical algorithms to extract and transform deep, imperceptible imaging features [27]. Studies have shown that radiomics based on image features can extract objective characteristics and provide valuable insights in predicting clinical outcomes [28].Indeed, both domestic and international researchers have been exploring the clinical utility of radiomics in diagnosing hepatic steatosis. For example, Chou and colleagues classified the severity of hepatic steatosis using patient ultrasound images [29, 30], while Sim and others used radiomics derived from MR-PDFF to diagnose the degree of hepatic fat deposition in NAFLD patients [31]. Ultrasound grayscale images indeed contain a wealth of raw image information, including reflections and scattering of small structures within the liver parenchyma [32]. In this study, ultrasound radiomics was used to extract image features from these grayscale ultrasound images. After dimension reduction using LASSO, a total of 25 features were retained, and a radiomics model was developed using the KNN algorithm. This radiomics model achieved an AUC of 0.967 in the training dataset and an AUC of 0.850 in the validation dataset.

The radiomics model outperformed the clinical model in both the training and validation datasets with AUC values greater than the clinical model. Furthermore, the clinical radiomics model developed using the LightGBM algorithm exhibited even better performance, achieving an AUC of 0.989 in the training dataset and an AUC of 0.885 in the validation dataset.The DeLong test showed that in the training dataset, the clinical radiomics model performed better than the clinical model ($p=0.013$), indicating that including radiomics factors improved predictive performance. Although there was no statistically significant difference between the clinical radiomics model and the radiomics model in the training dataset ($p=0.169$), there was no statistically significant difference in the validation dataset between the clinical radiomics model and the clinical model ($p=0.369$) or the radiomics model ($p=0.508$). However, the clinical radiomics model had higher AUC and accuracy than the other two models. DCA showed that within the threshold probability range of > 65%, the clinical radiomics model had the highest net benefit. The calibration curve in the validation dataset indicated that the clinical radiomics model was the best method for diagnosing NASH.The above findings suggest that the clinical radiomics model, which combines clinical features, elasticity imaging, and radiomic features extracted from ultrasound, can further improve the diagnostic performance of NASH. This can potentially reduce the need for unnecessary biopsies and provide strong evidence for clinicians to diagnose NASH and initiate early intervention and treatment.The idea of combining radiomics with clinical information for better diagnostic assistance in various clinical settings has been validated by previous studies, including those conducted by Huang YQ et al. and Meng F et al. [21, 33]. This supports the notion that radiomics, when integrated with clinical data, can enhance diagnostic capabilities across different clinical scenarios.

While our study provides promising results, it is important to acknowledge several limitations.Sample Size: The size of the animal model used in this study may not fully represent the complexity and variability seen in human patients with NASH. Expanding the study to a larger and more diverse sample, including human subjects, would enhance the generalizability of the findings.Data Collection: The data used in this study were collected from animal models, and there may be variations between animal and human physiology. Future studies should incorporate human data to validate the model's performance in a clinical setting. Model Validation: Although the models showed promising performance in the validation set, external validation using independent datasets from different sources or populations is essential to assess the model's robustness and generalizability.Our future plan is to collect clinical patient cases to use ultrasound imaging data. We will utilize a pre-trained radiomic models to automatically analyze liver conditions and identify potential NASH cases.

Conclusions

In conclusion, this animal study demonstrates that we have successfully established a model combining radiomics and clinical features, which can effectively predict the diagnosis of NASH.

This model provides potential opportunities for timely and effective therapeutic interventions, but further research is needed to validate its applicability and feasibility in human patients. This study offers valuable insights for the development of more accurate methods in the diagnosis and management of NASH in the future.

Supplementary Information

The online version contains supplementary material available at https://doi.org/10.1186/s12880-024-01398-y.

Supplementary Material 1.

Authors' contributions

Contributions: (I) Conception and design: F. X.; (II) Administrative support: C.Z.; (III) Provision of study materials: J.W. (IV) Collection and assembly of data: K.W.and F.X; (V) Data analysis and interpretation: F.X.andW.W.; (VI) Manuscript writing: All authors; (VII) Final approval of manuscript: All authors.

Funding

This work was supported by the institutional research project fund of the Second People's Hospital of Wuhu City, Anhui Province (JC2023B05).

Availability of data and materials

The data that support the findings of this study are available from the corresponding author upon reasonable request.

Data types and formats

• The types of data include raw experimental data, processed data.
• Data are available in Excel formats.

Supporting materials

• Additional supporting materials such as codebooks and analysis scripts are available from the corresponding author upon request.

Data Availability

Data is provided within the supplementary information and manuscript.

Declarations

Ethics approval and consent to participate

This study was approved by the Clinical Medicine Research Ethics Committee of the First Affiliated Hospital of Anhui Medical University, China, and complies with the National Guidelines for Animal Care and Use in China. Ethics approval number: 5101114.

Consent for publication

Not applicable. Since our research does not involve human subjects, publication consent is not applicable.

Competing interests

The authors declare no competing interests.

Received: 18 February 2024 Accepted: 12 August 2024
Published online: 20 August 2024

References

1. Nguyen TN, Podkowa AS, Tam AY, Arnold EC, Miller RJ, Park TH, Do MN, Oelze ML. Characterizing fatty liver in vivo in rabbits, using quantitative ultrasound. Ultrasound Med Biol. 2019;45(8):2049–62. https://doi.org/10.1016/j.ultrasmedbio.2019.03.021.
2. Papatheodoridi M, Cholongitas E. Diagnosis of Non-alcoholic Fatty Liver Disease (NAFLD): current concepts. Curr Pharm Des. 2018;24(38):4574–86. https://doi.org/10.2174/1381612825666190117102111.
3. Sheka AC, Adeyi O, Thompson J, Hameed B, Crawford PA, Ikramuddin S. Nonalcoholic steatohepatitis: a review [published correction appears in JAMA. 2020 Apr 28;323(16):1619]. JAMA. 2020;323(12):1175–83. https://doi.org/10.1001/jama.2020.2298.
4. Schuster S, Cabrera D, Arrese M, Feldstein AE. Triggering and resolution of inflammation in NASH. Nat Rev Gastroenterol Hepatol. 2018;15(6):349–64. https://doi.org/10.1038/s41575-018-0009-6.
5. Petta S, Handberg A, Craxì A. Non invasive indexes for the assessment of patients with non-alcoholic fatty liver disease. Curr Pharm Des. 2013;19(29):5193–218 PMID: 23394090.
6. Houghton D, Zalewski P, Hallsworth K, Cassidy S, Thoma C, Avery L, Slomko J, Hardy T, Burt AD, Tiniakos D, Hollingsworth KG, Taylor R, Day CP, Masson S, McPherson S, Anstee QM, Newton JL, Trenell MI. The degree of hepatic steatosis associates with impaired cardiac and autonomic function. J Hepatol. 2019;70(6):1203–13. https://doi.org/10.1016/j.jhep.2019.01.035.
7. Brunt EM. Pathology of fatty liver disease. Mod Pathol. 2007;20(Suppl 1):S40–8. https://doi.org/10.1038/modpathol.3800680.
8. Kang BK, Kim M, Song SY, Jun DW, Jang K. Feasibility of modified Dixon MRI techniques for hepatic fat quantification in hepatic disorders: validation with MRS and histology. Br J Radiol. 2018;91(1089):20170378. https://doi.org/10.1259/bjr.20170378.
9. Ferraioli G, Maiocchi L, Raciti MV, Tinelli C, De Silvestri A, Nichetti M, De Cata P, Rondanelli M, Chiovato L, Calliada F, Filice C. Detection of liver steatosis with a novel ultrasound-based technique: a pilot study using MRI-derived proton density fat fraction as the gold standard. Clin Transl Gastroenterol. 2019;10(10):e00081. https://doi.org/10.14309/ctg.0000000000000081.
10. Salman AA, Aboelfadl SA, Heagzy MA. New era for usage of serum liver enzymes as a promising horizon for the prediction of non-alcoholic fatty liver disease. Open Access Maced J Med Sci. 2016;4(3):348–52. https://doi.org/10.3889/oamjms.2016.092.
11. Pulzi FB, Cisternas R, Melo MR, Ribeiro CM, Malheiros CA, Salles JE. New clinical score to diagnose nonalcoholic steatohepatitis in obese patients. Diabetol Metab Syndr. 2011;3(1):3. https://doi.org/10.1186/1758-5996-3-3.Published 2011 Feb 23.
12. Hu W, Yang H, Xu H, Mao Y. Radiomics based on artificial intelligence in liver diseases: where we are? Gastroenterol Rep (Oxf). 2020;8(2):90–7. https://doi.org/10.1093/gastro/goaa011. Published 2020 Apr 7.
13. Van Herck MA, Vonghia L, Francque SM. Animal models of nonalcoholic fatty liver disease-a starter's guide. Nutrients. 2017;9(10):1072. https://doi.org/10.3390/nu9101072.
14. Kubota N, Kado S, Kano M, Masuoka N, Nagata Y, Kobayashi T, Miyazaki K, Ishikawa F. A high-fat diet and multiple administration of carbon tetrachloride induces liver injury and pathological features associated with non-alcoholic steatohepatitis in mice. Clin Exp Pharmacol Physiol. 2013;40(7):422–30. https://doi.org/10.1111/1440-1681.12102.
15. Bingül İ, Aydın AF, Başaran-Küçükgergin C, Doğan-Ekici I, Çoban J, Doğru-Abbasoğlu S, Uysal M. High-fat diet plus carbon tetrachloride-induced liver fibrosis is alleviated by betaine treatment in rats. Int Immunopharmacol. 2016;39:199–207. https://doi.org/10.1016/j.intimp.2016.07.028.
16. Turkay R, Aydin AF, Bingul I, Kucukgergin C, Dogan-Ekici I, Hocaoglu E, Inci E, Bakir B, Uysal M. Can ultrasound imaging predict the success of an experimental steatofibrosis model? Ultrasound Q. 2017;33(2):157–61. https://doi.org/10.1097/RUQ.0000000000000286.
17. Castera L, Friedrich-Rust M, Loomba R. Noninvasive assessment of liver disease in patients with nonalcoholic fatty liver disease. Gastroenterology. 2019;156(5):1264-1281.e4. https://doi.org/10.1053/j.gastro.2018.12.036.
18. Castera L, Pawlotsky JM. Noninvasive diagnosis of liver fibrosis in patients with chronic hepatitis C. MedGenMed. 2005;7(4):39 PMID: 16614661; PMCID: PMC1681713.
19. Ohara M, Ohnishi S, Hosono H, Yamamoto K, Yuyama K, Nakamura H, Qingjie Fu, Maehara O, Suda G, Sakamoto N. Extracellular vesicles from amnion-derived mesenchymal stem cells ameliorate hepatic inflammation and fibrosis in rats. Stem Cells Int. 2018;2018:3212643. https://doi.org/10.1155/2018/3212643. Published 2018 Dec 24.
20. Zheng YP, Zhong XY, Huang YS, Zheng CB. HCBP6 Is involved in the development of hepatic steatosis induced by high-fat diet and CCL4 in rats. Ann Hepatol. 2018;17(3):511–8. https://doi.org/10.5604/01.3001.0011.7396.
21. Meng F, Wu Q, Zhang W, Hou S. Application of interpretable machine learning models based on ultrasonic radiomics for predicting the risk of fibrosis progression in diabetic patients with nonalcoholic fatty liver disease. Diabetes Metab Syndr Obes. 2023;16:3901–13. https://doi.org/10.2147/DMSO.S439127. Published 2023 Dec 2.
22. Vilar-Gomez E, Martinez-Perez Y, Calzadilla-Bertot L, Torres-Gonzalez A, Gra-Oramas B, Gonzalez-Fabian L, Friedman SL, Diago M, Romero-Gomez M. Weight loss through lifestyle modification significantly reduces features of nonalcoholic steatohepatitis. Gastroenterology. 2015;149(2):367-e15. https://doi.org/10.1053/j.gastro.2015.04.005.

23. Younossi ZM, Koenig AB, Abdelatif D, Fazel Y, Henry L, Wymer M. Global epidemiology of nonalcoholic fatty liver disease-Meta-analytic assessment of prevalence, incidence, and outcomes. Hepatology. 2016;64(1):73–84. https://doi.org/10.1002/hep.28431.
24. Morin J, Swanson TA, Rinaldi A, Boucher M, Ross T, Hirenallur-Shanthappa D. Application of ultrasound and shear wave elastography imaging in a rat model of NAFLD/NASH. J Vis Exp. 2021;(170). Published 2021 Apr 20. https://doi.org/10.3791/62403
25. Gao J, Wong C, Maar M, Park D. Reliability of performing ultrasound derived SWE and fat fraction in adult livers. Clin Imaging. 2021;80:424–9. https://doi.org/10.1016/j.clinimag.2021.08.025.
26. Tang A, Destrempes F, Kazemirad S, Garcia-Duitama J, Nguyen BN, Cloutier G. Quantitative ultrasound and machine learning for assessment of steatohepatitis in a rat model. Eur Radiol. 2019;29(5):2175–84. https://doi.org/10.1007/s00330-018-5915-z.
27. Jia Yingying, Yang Jun, Zhu Yangyang, Nie Fang, Haoao Wu, Duan Ying, Chen Kundi. Ultrasound-based radiomics: current status, challenges and future opportunities. Med Ultrason. 2022;24(4):451–60. https://doi.org/10.11152/mu-3248.
28. Li F, Pan D, He Y, Wu Y, Peng J, Li J, Wang Y, Yang H, Chen J. Using ultrasound features and radiomics analysis to predict lymph node metastasis in patients with thyroid cancer. BMC Surg. 2020;20(1):315. https://doi.org/10.1186/s12893-020-00974-7. Published 2020 Dec 4.
29. Cao LL, Peng M, Xie X, Chen GQ, Huang SY, Wang JY, Jiang F, Cui XW, Dietrich CF. Artificial intelligence in liver ultrasound. World J Gastroenterol. 2022;28(27):3398–409. https://doi.org/10.3748/wjg.v28.i27.3398.
30. Chou T-H, Yeh H-J, Chang C-C, Tang J-H, Kao W-Y, Su I-C, Li C-H, Chang W-H, Huang C-K, Sufriyana H, Su EC-Y. Deep learning for abdominal ultrasound: A computer-aided diagnostic system for the severity of fatty liver. J Chin Med Assoc. 2021;84(9):842–50. https://doi.org/10.1097/JCMA.0000000000000585.
31. Sim KC, Kim MJ, Cho Y, Kim HJ, Park BJ, Sung DJ, Han NY, Han YE, Kim TH, Lee YJ. Radiomics analysis of magnetic resonance proton density fat fraction for the diagnosis of hepatic steatosis in patients with suspected non-alcoholic fatty liver disease. J Korean Med Sci. 2022;37(49):e339. https://doi.org/10.3346/jkms.2022.37.e339.Published 2022 Dec 19.
32. Xue L-Y, Jiang Z-Y, Tian-Tian Fu, Wang Q-M, Zhu Y-L, Dai M, Wang W-P, Jin-Hua Yu, Ding H. Transfer learning radiomics based on multimodal ultrasound imaging for staging liver fibrosis. Eur Radiol. 2020;30(5):2973–83. https://doi.org/10.1007/s00330-019-06595-w.
33. Huang YQ, Liang CH, He L, Tian J, Liang CS, Chen X, Ma ZL, Liu ZY. Development and Validation of a Radiomics Nomogram for Preoperative Prediction of Lymph Node Metastasis in Colorectal Cancer [published correction appears in J Clin Oncol 2016 Jul 10;34(20):2436]. J Clin Oncol. 2016;34(18):2157–64. https://doi.org/10.1200/JCO.2015.65.9128.

Publisher's Note